Supplementary table

Table S1. Linear trends of solutes in µmol kg^{-1} yr^{-1} with 95% confidence intervals where data are available for the entire period since 1950, for negative (1950-1976; PDO-) and positive (after 1976; PDO+) PDO periods in the 50 to 300 m depth layer for April to December measurements for area P (48°-52°N, 143°-147°W) and Oyashio region (39°-42°N, 144°-149°E).

Parameter	trend	time period	PDO- trend	time period	PDO+ trend	time period
Area		area P		area P		area P
Oxygen	*-0.22± 0.23*	1954-2017	*-0.16 ± 1.44*	1954-1976	*-0.22 ± 0.43*	1977-2017
Nitrate	+0.069 ± 0.050	1956-2017	*-0.114 ± 0.516*	1956-1973	+0.069 ± 0.050	1980-2017
Silicate	+0.491 ± 0.177	1958-2017	*+2.26 ± 5.74*	1958-1971	+0.216 ± 0.211	1987-2017
Phosphate	*+0.001 ± 0.003*	1954-2017	*-0.014 ± 0.025*	1954-1971	*+0.001 ± 0.007*	1980-2017
Area		Oyashio region		Oyashio region		Oyashio region
Oxygen	*-0.18 ± 0.32*	1952-2017	*-0.27 ± 0.56*	1952-1976	*+0.14 ± 0.72*	1977-2017
Nitrate	+0.106 ± 0.043	1964-2017	*+0.365 ± 0.566*	1964-1976	+0.124 ± 0.060	1977-2017
Silicate	*+0.156 ± 0.340*	1952-2017	-1.40 ± 1.14	1952-1971	+0.614 ± 0.343	1981-2017
Phosphate	+0.006 ± 0.003	1953-2017	*+0.011 ± 0.017*	1953-1976	*+0.009 ± 0.005*	1977-2017

22

23

24

25

26

Supplementary figures
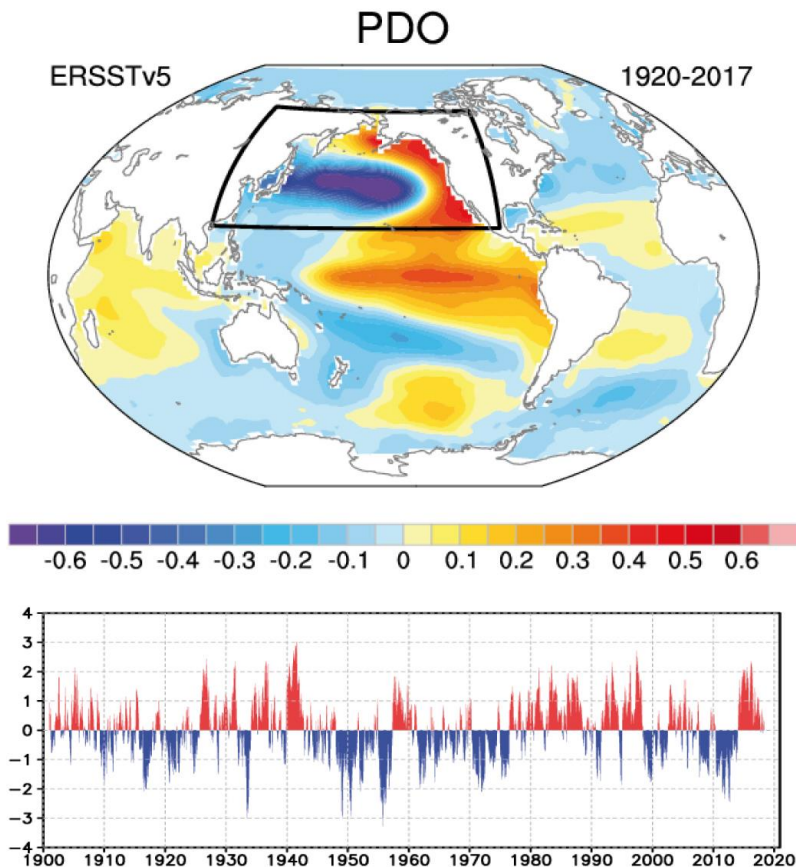
Figure S1. Global expression of the Pacific Decadal Oscillation (PDO, top) obtained by linearly regressing monthly sea surface temperature (SST) anomalies (in °C) based on ERSSTv5 data set (Huang et al., 2017) for the period 1920-2017 at each grid box upon the leading Principal Component (PC) time series based on the domain outlined in the black box (Adapted from Deser et al., 2010 and modified by A. Phillips). The PDO time series 1900 to 2017, defined by their corresponding PC is shows in the lower frame. (Figure from Tokyo Climate Center, http://ds.data.jma.go.jp/tcc/tcc/products/elnino/decadal/pdo_month.html) based on the HadlSST data set (Rayner et al., 2003).
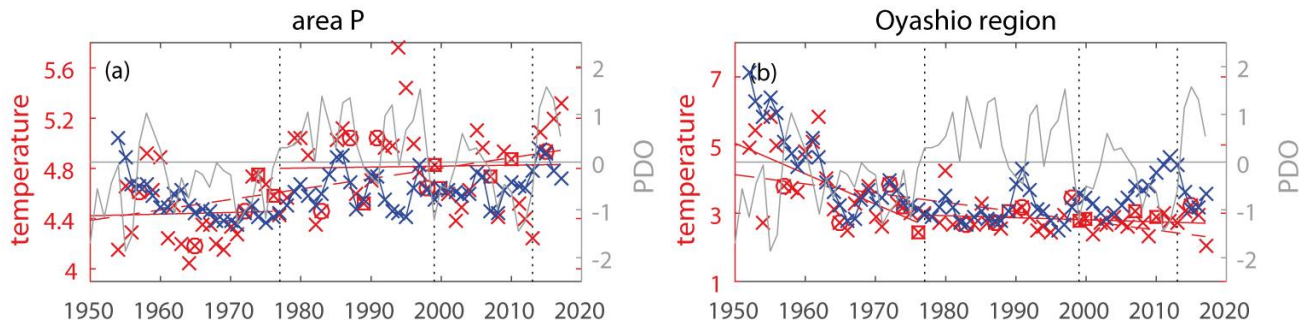
6 **Figure S2.** Annual mean concentration of temperature in °C for years available and trends for the
7 layer 50 to 300 m plotted for the entire time period (dashed red lines) and for the periods 1950 to
8 1976 for the negative PDO phase and after 1976 for the positive PDO phase (solid red lines) a) at
9 area P (48° to 52°N, 143° to 147°W) from hydrodata CTD and bottle data and station P data (50°N,
10 145°W) for the period 1954 to 2017 with a trend of 0.0083 +/- 0.0073 °C yr^{-1} and b) the Oyashio
11 region between 39° and 42°N, 144° and 149°E for the period 1952 to 2017 with a trend of -0.0273+/-
12 0.0188 °C yr^{-1}. El Niño years defined as strong are marked by an additional circle, strong La Niña
13 years by an additional square. The change of the PDO status in 1977, 1999 and 2013 are marked by
14 vertical dotted lines. PDO annual time series are shown in the temperature time series as solid grey
15 lines. In addition the annual mean 0 to 50 m temperatures smoothed with a 4-point running mean are
16 included as blue lines covering the temperature range 6.0 to 10.2 °C in area P and 5.3 to 16.4°C in the
17 Oyashio region.

18

19

20

21

22

23

24

25

26

27
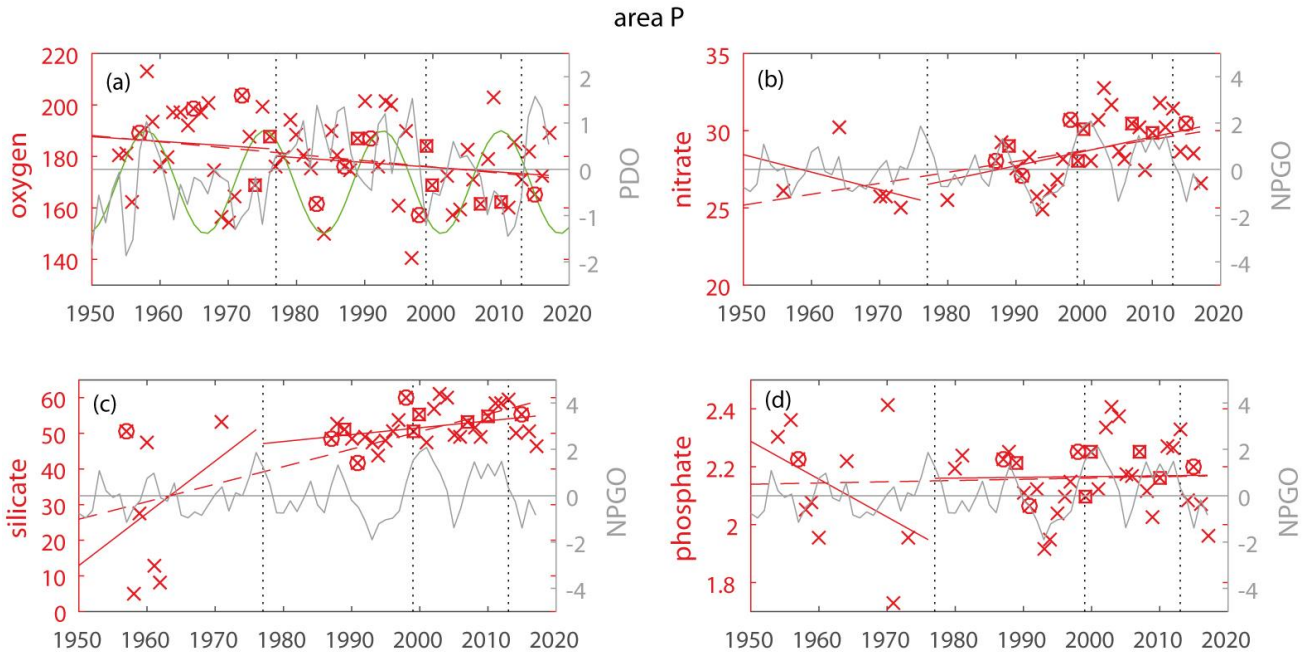
Figure S3. Annual mean concentration for years available and trends for the layer 50 to 300 m plotted for the entire time period (dashed red lines) and for the periods 1950 to 1976 for the negative PDO phase and after 1976 for the positive PDO phase (solid red lines) at area P (48° to 52°N, 143° to 147°W) from hydrodata CTD and bottle data and station P data (50°N, 145°W) for the period since 1956 in µmol kg^{-1} yr^{-1} for a) oxygen, b) nitrate, c) silicate and d) phosphate. For oxygen measurements in 2001 were removed as the 50-300 m mean was much to high (379 µmol kg^{-1}). El Niño years defined as strong are marked by an additional circle, strong La Niña years by an additional square. The change of the PDO status in 1977, 1999 and 2013 are marked by vertical dotted lines. The PDO annual mean time series are shown in the oxygen time series and the NPGO annual mean time series in nitrate, phosphate and silicate time series as solid grey lines. In the oxygen time series the 18.6 year sinusoidal nodal cycle is included (green curve).
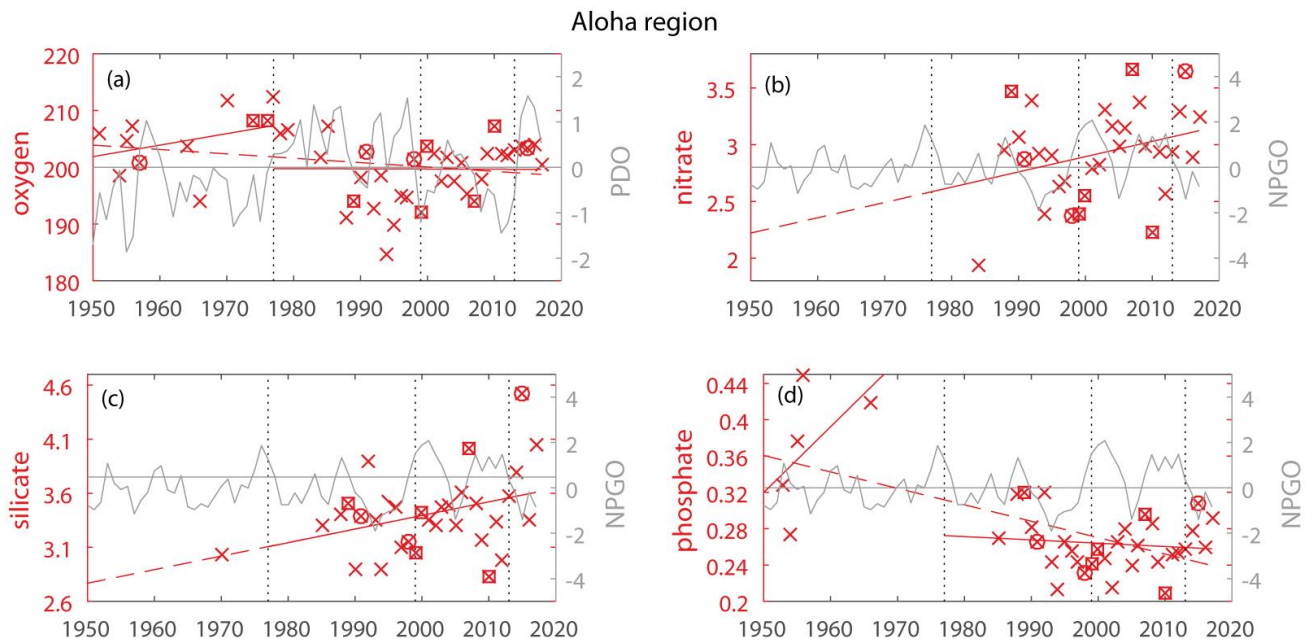
Figure S4. Annual mean concentration for years available and trends for the layer 50 to 300 m plotted for the entire time period (dashed red lines) and for the periods 1950 to 1976 for the negative PDO phase after 1976 for the positive PDO phase (solid red lines) between 22° and 25°N, 156 and 159°W from hydrodata CTD and bottle data and station Aloha data (22°45'N, 158°W) for the period since October 1988 in µmol kg^{-1} yr^{-1} for a) oxygen, b) nitrate, c) silicate and d) phosphate. For silicate measurements in 1984 were removed as they were to low (1.83 µmol kg^{-1}) phosphate measurements in 1951 were removed as the 50-300 m mean was to high (0.573 µmol kg^{-1}). El Niño years defined as strong are marked by an additional circle, strong La Niña years by an additional square. The change of the PDO status in 1977, 1999 and 2013 are marked by vertical dotted lines. PDO annual mean time series are shown in the oxygen time series and the NPGO annual mean time series in nitrate, phosphate and silicate time series as solid grey lines.

Peru region
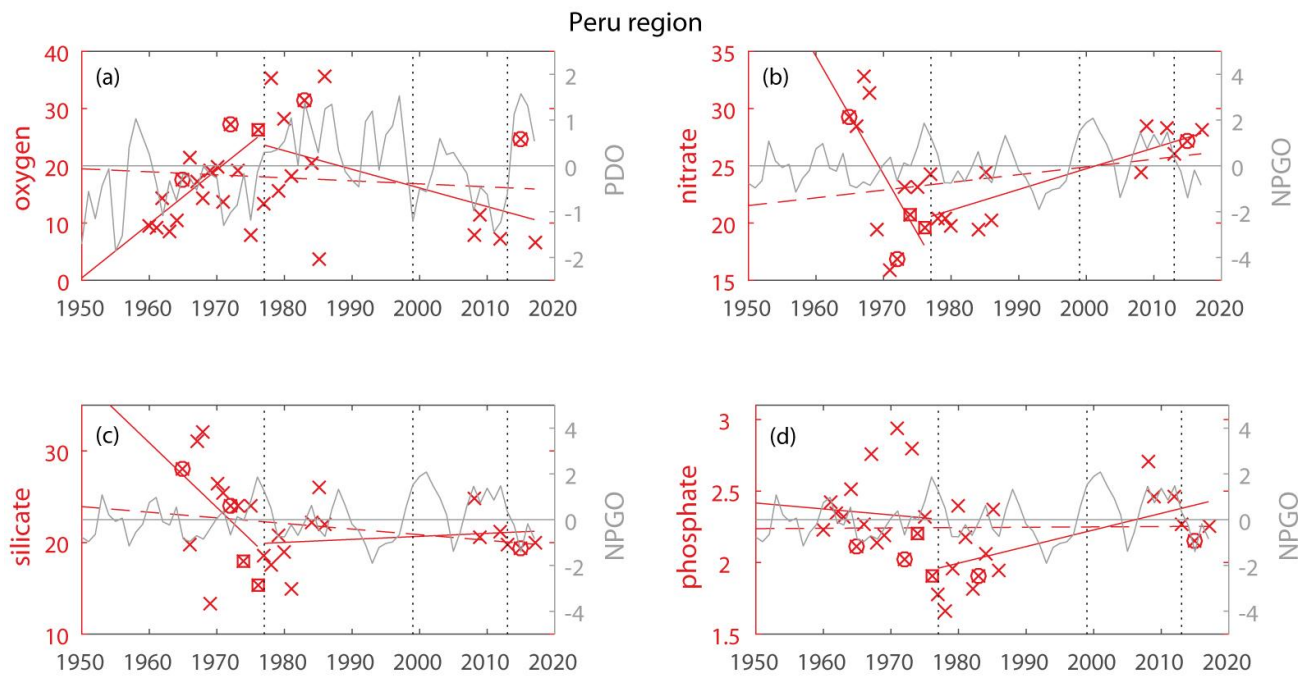
Figure S5. Annual mean concentration for years available and trends for the layer 50 to 300 m
plotted for the entire time period (dashed red lines) and for the periods 1950 to 1976 for the negative
PDO phase and after 1976 for the positive PDO phase (solid red lines) between 7° and 12°S, 78 and
83°W from hydrodata CTD and bottle data in µmol kg^{-1} yr^{-1} for a) oxygen, b) nitrate, c) silicate and
d) phosphate. For oxygen measurements in 1982 were removed as they were to high (62.4 µmol kg^{-1}). El Niño years defined as strong are marked by an additional circle, strong La Niña years by an
additional square. The change of the PDO status in 1977, 1999 and 2013 are marked by vertical
dotted lines. PDO annual mean time series are shown in the oxygen time series and the NPGO annual
mean time series in the nitrate, silicate and phosphate time series as solid grey lines.

Supplementary references:

Deser, C., Alexander, M. A., Xie, S.-P., and Phillips, A. S.: Sea surface temperature variability:
Patterns and mechanisms, Annu. Rev. Mar. Sci., 2, https://doi.org/10.1146/annurev-marine-120408-
151453, 2010.

Huang, B., Thorne, P. W., Banzon, V. F., Boyer, T., Cherupin, G., Lawrimore, J. H., Menne, M. J.,
Smith, T. M., Vose, R. S., and Zhang, H.-M.: Extended reconstructed sea surface temperature,
version 5 (ERSSTv5): Upgrades, validations, and intercomparisons, J. Climate, 30,
https://doi.org/10.1175/JCLI-D-16-0836.1, 2017.

1   Rayner, N. A., Parker, D. E., Horton, E. B., Folland, C. K., Alexander, L. V., Rowell, D. P., Kent, E.

2   C., and Kaplan, A.: Global analyses of sea surface temperature, sea ice, and night marine air

3   temperature since the late nineteenth century, J. Geophys. Res. 108 D14, 4407,

4   https://doi.org/10.1029/2002JD002670, 2003.